Green Chemistry

PAPER

View Article Online
View Journal

Cite this: DOI: 10.1039/c8gc02527d

Ultrafine hybrid Cu_2O–Fe_2O_3 nanoparticles stabilized by hexaphenylbenzene-based supramolecular assemblies: a photocatalytic system for the Ullmann–Goldberg coupling reaction†

Gurpreet Singh, Manoj Kumar * and Vandana Bhalla *

Received 10th August 2018,
Accepted 22nd October 2018

DOI: 10.1039/c8gc02527d

rsc.li/greenchem

Ultrafine hybrid Cu_2O–Fe_2O_3 NPs have been prepared using the supramolecular assemblies of hexaphenylbenzene (HPB) derivative **3** as nanoreactors and stabilizers. The as-prepared hybrid Cu_2O–Fe_2O_3 NPs serve as an efficient and recyclable photocatalytic system for carrying out C–N coupling between aryl halides and various amines (aliphatic, aromatic and N-heterocyclic) at room temperature in mixed aqueous media under visible light irradiation. Amazingly, Cu_2O–Fe_2O_3 NPs also exhibited high efficiency in the reactions involving the synthesis of biologically important *N*-substituted carbazole derivatives. The work being presented in this article demonstrates the preparation of a 'dip strip' coated with the as-prepared catalytic system and utilization of this paper strip as a recyclable and portable heterocatalytic system for carrying out the Ullmann–Goldberg coupling.

Introduction

The development of facile methods for introducing nitrogen functionality into organic frameworks has been one of the major research topics in synthetic organic chemistry owing to the ubiquity of heterocyclic compounds in natural products and medicinally important derivatives.[1–5] Conventionally, palladium-catalyzed Buchwald–Hartwig coupling of amines and aryl halides is a powerful tool for the synthesis of N-heterocyclic compounds.[6] Although this method of amination is efficient, the reaction conditions require an inert atmosphere, high temperature and high loading of the palladium catalyst for obtaining the target molecule in good to excellent yields. For making this coupling reaction eco-friendly, a variety of catalytic systems based on transition metal ions such as gold,[7] copper,[8–11] nickel,[12–14] cobalt[15–19] and zinc[20] have been developed over the last decade. Despite the different beneficial aspects of these reported catalytic systems, it was not possible to overcome the requirement of high temperature, presence of additional ligands, high equivalents of bases and organic solvents as the reaction media. Further, the use of stoichiometric amounts of metal reagents such as CuI restricted the large scale industrial application of these reported systems.[21] Thus, the development of new sustainable and green synthetic methods for carrying out C–N coupling is a challenge yet to be achieved.

Our research work involves the development of supramolecular ensembles having metal nanoparticles as catalytic centers for carrying out various carbon–carbon and carbon–heteroatom bond formation reactions under mild conditions.[23–27] In continuation of our efforts in this direction, we were then interested in the development of more efficient, greener, recyclable and economical catalytic systems for C–N bond formation. In the literature, several research groups have reported the utilization of benign, economical copper metal-based catalytic systems for carrying out C–N bond formation reactions, which work efficiently only under an inert atmosphere at a high temperature in the presence of additives and organic solvents.[8–11,28] Recently, an Ir/Cu-based photocatalytic system has been reported for carrying out C–N coupling reaction in organic solvents under the irradiation of a blue LED and in the presence of a strong organic base[22] (Scheme 1A). These reports inspired us to develop a copper-based photocatalytic system which could overcome the limitations of previously reported systems such as the inert atmosphere, presence of additives, organic solvents and utilization of a blue

Department of Chemistry, UGC Sponsored Centre for Advanced Studies-II, Guru Nanak Dev University, Amritsar 143005, Punjab, India.
E-mail: vanmanan@yahoo.co.in, mksharmaa@yahoo.co.in

†Electronic supplementary information (ESI) available: The contents of the ESI section include ^{1}H, ^{13}C NMR and ESI-MS spectra of compounds; UV-vis and SEM and TEM images; powder XRD analysis; VSM analysis; DLS studies; XPS studies; and IR spectroscopy. See DOI: 10.1039/c8gc02527d

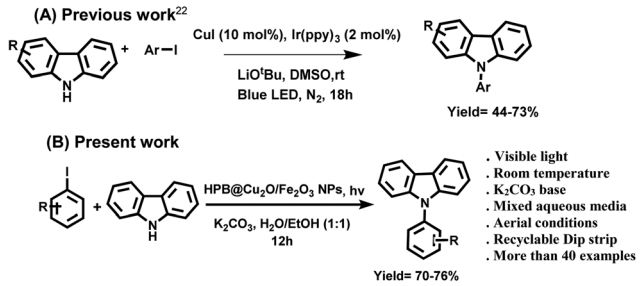

Scheme 1 Photocatalytic systems for the Ullmann–Goldberg coupling reaction.

LED as the radiation source for carrying out C–N bond formation reactions. We envisioned that a supramolecular ensemble developed in mixed aqueous media having copper as the catalytic center and supramolecular assemblies as the visible light harvesting centers could be a good choice for the preparation of an efficient catalytic system for carrying out C–N bond formation reactions under mild conditions. For the development of such a photocatalytic system, we planned to have a hexaphenylbenzene (HPB) core as the scaffold of the supramolecular assemblies. HPB derivatives are known to emit in the wavelength range of 400–550 nm (ref. 29 and 30); hence, a good overlap is expected between the emission spectrum of the HPB derivative and the absorption spectrum of Cu_2O NPs, which is a must for possible energy transfer between supramolecular assemblies and metal NPs during the photocatalytic process. Recently, we have reported Ag@Cu_2O core–shell NPs stabilized by the supramolecular assemblies of HPB derivative **1** (Chart 1) and utilized them as an efficient photocatalytic system for carrying out C–H activation reactions.[31]

As a test of our hypothesis, we planned to examine the applicability of this system for carrying out C–N bond formation reactions under photocatalytic conditions. We chose the reaction between iodobenzene and morpholine as the model reaction. The reaction proceeded; however, the target product was obtained only in 40% yield (*vide infra*). This study suggests that the Ag@Cu_2O system is not an efficient catalytic system for C–N bond formation. We envisaged that by switching Ag NPs with some other metallic species which could assist Cu_2O in C–N bond formation reactions, the yield of the target compound may be improved. Among all the other metal ions, the iron metal ion is of our choice as the catalytic partner of copper due to its known catalytic efficiency in C–N bond formation.[32] We further expected that the presence of magnetically active iron species in bimetallic magnetic nanocomposites will improve the recyclability of the catalytic system in C–N bond formation reactions. Unfortunately, the photophysical properties of derivative **1** remained unchanged in the presence of ferric ions. To enhance the affinity of the HPB derivative towards iron, we introduced morpholine groups at the periphery of the molecule through imine linkages. Morpholine moieties are known to have affinity toward ferric ions.[33] We envisaged that morpholine groups along with imine linkages will enhance the affinity of the molecule towards Fe^{3+} and Cu^{2+} ions. As expected, derivative **3** formed spherical fluorescent supramolecular aggregates in the mixed aqueous media, which exhibited sensitive response toward Cu^{2+} and Fe^{3+} ions and served as reactors and stabilizers for the preparation of ultrafine hybrid Cu_2O–Fe_2O_3 NPs. Further, supramolecular aggregates of the HPB derivative in combination with hybrid Cu_2O–Fe_2O_3 NPs act as efficient photocatalysts for Ullmann–Goldberg coupling under mild conditions (Scheme 1B). The photocatalytic system being presented in this article has several advantages over the literature reports (Table S1 in the ESI†). First, the aggregates of derivative **3** act as nanoreactors for the preparation of ultrafine nanomaterials in the absence of any additional reducing and stabilizing agents. Previously, there were a few reports for the preparation of Cu_2O–Fe_2O_3 alloy NPs;[34,35] however, these methods involve the utilization of harsh conditions such as the use of reducing/capping agents, organic solvents, high temperature, longer reaction time and an inert atmosphere to yield the Cu_2O–Fe_2O_3 alloy NPs (Table S2 in the ESI†) of bigger size. In this context, the method being reported in this article is convenient, fast and 'green'. We believe that the preparation of ultrafine (5–7 nm) Cu_2O–Fe_2O_3 magnetic nanocomposites is unprecedented in the literature. Additionally, during the formation of nanomaterials, the imine linkages were hydrolyzed, which restored the aldehyde groups at the periphery of derivative **3**. To the best of our knowledge, this is the first report of alloy nanoparticle induced hydrolysis of the Schiff base to generate the aggregates of the HPB derivative having aldehyde groups at their periphery. Second, the as-prepared ultrafine hybrid Cu_2O–Fe_2O_3 nanoparticles act as an efficient catalytic system for carrying out the visible light mediated C–N coupling reaction of aromatic halides with various amines (primary/secondary aliphatic, aromatic and N-heterocyclic amines). Additionally, being magnetic in nature, the separation of the present catalytic system was very easy and it exhibited recyclability for six runs. The good recyclability of the catalytic system clearly demonstrates the efficiency of the supramolecular aggregates in preventing the leaching of nanomaterials. Previously, palladium- and CuI-based catalytic systems have been used for carrying out reactions between aryl halides and aliphatic amines. However, these reactions required the presence of strong bases such as NaO^{t}Bu, Cs_2CO_3, ligands, organic solvents (DMSO, DMF, isopropanol, and toluene), high temperature and longer reaction time.[28,36–39] Third, most importantly, the as-prepared catalytic system exhibited high efficiency in the preparation of *N*-substituted carbazoles. The

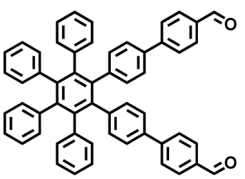

Chart 1 Structure of HPB derivative **1**.

development of simple and efficient methods for the preparation of *N*-substituted derivatives of carbazole is important due to the potential applications of these compounds as building blocks for the preparation of molecules having material and pharmaceutical applications. In the literature, an iridium-based complex has been used as a photocatalyst for carrying out *N*-arylation of carbazoles under strong basic conditions using DMSO as a solvent under a blue LED and inert atmosphere for a prolonged reaction time (18 h).[22] Very recently, an Ir/Ni-based catalytic system has been reported which could not catalyze the reaction involving amines lacking in α-hydrogens even in the presence of DABCO as the base and DMSO as the solvent.[12] In contrast to this, the as-prepared Cu_2O–Fe_2O_3 nanocatalytic system works efficiently in mixed aqueous media under mild reaction conditions and requires a shorter reaction time period (6 h) for the completion of the reaction. Fourth, the 'dip strip' prepared by dipping a filter paper strip into the solution of a supramolecular ensemble worked as a heterocatalytic system for carrying out C–N bond formation reactions. The dried coated strip could be reused as a heterocatalytic system for carrying out C–N bond formation reactions up to three cycles.

Results and discussion

Synthesis and characterization of hexaphenylbenzene derivative 3

Condensation of HPB derivative **1** [40] with 4-(2-aminoethyl)morpholine **2** in dichloromethane (DCM)/ethanol (EtOH) (2 : 8) furnished compound **3** in 75% yield (Scheme 2). The structure of compound **3** was confirmed from its spectroscopic data. The ^{1}H NMR spectrum of compound **3** showed one singlet at 8.26 ppm corresponding to imino protons, four doublets at 7.66, 7.47, 7.17, and 6.94 ppm corresponding to aromatic protons, two multiplets – one at 6.86–6.85 ppm corresponding to aromatic protons and another at 3.78–3.69 ppm corresponding to methylene protons, two triplets at 2.70 and 2.54 ppm corresponding to methylene protons. A parent ion peak for $[M + H]^+$ was observed at m/z = 967.4964 in the mass spectrum. The IR spectrum of derivative **3** showed characteristic peaks of C=N and C–N bonds at 1630 cm^{-1} and 1116 cm^{-1}, respectively. These spectroscopic data corroborate structure **3** for this compound (Fig. S75–S78 in the ESI†).

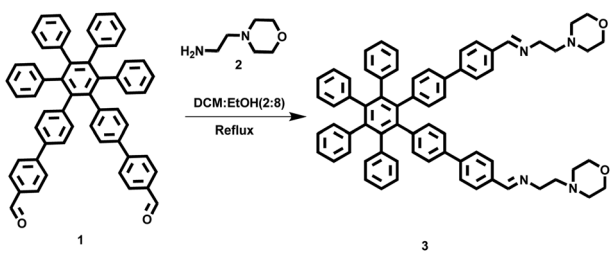

Scheme 2 Synthesis of hexaphenylbenzene-based derivatives **3**.

Photophysical properties of derivative 3

The UV-vis spectrum of derivative **3** in THF exhibits an absorption band at 305 nm due to the π–π* transition. On adding water fractions up to 90% (volume fraction) to the THF solution, the intensity of the absorption band increased with a slight red shift (~6 nm) from 305 to 311 nm (Fig. S1 in the ESI†). Further, a level-off tail was also observed in the visible region due to the formation of aggregates.[41] The THF solution of derivative **3** is non-emissive when excited at 305 nm; however, an emission band at 440 nm was observed on addition of 10% water fraction (Φ = 0.06) to the THF solution. On increasing the water fraction up to 60% (volume fraction), the emission band red-shifted to 455 nm with an enhancement in the emission intensity (Φ = 0.45) (Fig. S2 in the ESI†). We also studied the fluorescence behaviour of derivative **3** in different solvent mixtures of DMSO and glycerol. It was observed that upon increasing the volume fraction of glycerol from 0% to 99%, the emission intensity of derivative **3** was enhanced (Fig. S3 in the ESI†). This enhancement in the emission intensity upon increasing the viscosity of the solvent clearly suggests that the restriction to intramolecular rotation is the reason behind the aggregation induced emission enhancement (AIEE) phenomenon. The absorption and fluorescence studies suggest the formation of *J*-aggregates of derivative **3** in the mixed aqueous media. The concentration-dependent ^{1}H NMR studies of derivative **3** (Fig. S4 in the ESI†) show a slight down-field shift of all the aromatic protons, which also supports the formation of *J*-aggregates (Scheme 3). The transmission electron microscopy (TEM) image of compound **3** in H_2O/THF (6/4) showed the presence of spherical aggregates having an average size in the range of 400–450 nm (Fig. S5 in the ESI†) in the mixed aqueous media. The dynamic light scattering (DLS) studies also indicate the average size of aggregates in the range of 400–500 nm (Fig. S6 in the ESI†) in H_2O/THF (6/4) solvent mixture.

Preparation of ultrafine hybrid HPB@Cu_2O–Fe_2O_3 NPs

The presence of imino moieties and nitrogen atoms in derivative **3** prompted us to examine the binding ability of derivative **3** toward different metal ions, such as Zn^{2+}, Cu^{2+}, Hg^{2+}, Au^{3+}, Fe^{2+}, Fe^{3+}, Co^{2+}, Pb^{2+}, Pd^{2+}, Ni^{2+}, Cd^{2+}, Ba^{2+}, Mg^{2+}, Ag^{+}, and Al^{3+}as both their perchlorate and chloride salts using UV–vis spectroscopy. Upon gradual addition of Fe^{3+} ions (0–60 equiv.) to the solution of derivative **3** (5 μM) in H_2O/THF (6/4, v/v), a new absorption band at 500 nm was observed, which corresponds to the surface plasmon resonance (SPR) band of Fe_2O_3 nanoparticles[42] (Fig. S7 in the ESI†). The color of the solution changed from colorless to yellow, which was clearly visible to the naked eye. The TEM image of the solution showed the formation of the rod-shaped nanoparticles (Fig. S8 in the ESI†). Further, upon gradual addition of Cu^{2+} ions (0–120 equiv.) to the solution of derivative **3** (5 μM) in H_2O/THF (6/4, v/v), new absorption bands were observed at 258 and 715 nm, respectively, within 30 min (Fig. S9 in the ESI†). These absorption bands correspond to the surface plasmon resonance (SPR)

band of the Cu_2O nanoparticles.[43,44] The color of the solution changed from colorless to light reddish, which was clearly visible to the naked eye. The TEM image clearly shows the formation of spherical nanoparticles (Fig. S10 in the ESI†). No change in the absorption spectra was observed in the presence of other metal ions (Fig. S11 in the ESI†). In the fluorescence spectra, upon addition of 60 equiv. of Fe^{3+} ions to the solution of derivative **3** (5 μM) in the H_2O/THF (6/4, v/v) mixture, the intensity of the emission band at 455 nm gradually decreased (Fig. S12 in the ESI†). Likewise, upon addition of Cu^{2+} ions (120 equiv.) to the solution of aggregates of **3**, the intensity of the emission band at 455 nm gradually decreased (Fig. S13 in the ESI†). These spectral changes indicate the interactions between the aggregates of derivative **3**, Fe^{3+} ions and Cu^{2+} ions.

Keeping in mind the potential of the aggregates of derivative **3** to generate Cu_2O and Fe_2O_3 NPs, we planned to prepare hybrid nanoparticles of Cu_2O–Fe_2O_3 using the supramolecular assemblies of derivative **3** as a common platform. To the solution of supramolecular assemblies of derivative **3** in H_2O/THF (6/4, v/v), we added Cu^{2+} ions (0–120 equiv.) and Fe^{3+} ions (0–60 equiv.), simultaneously and kept the solution for 30 min at room temperature (Fig. 1B). The absorbance spectra of this solution showed the absorption bands at 258 nm and in the region of 700–750 nm characteristics of Cu_2O NPs. A broadband in the region of 490–530 nm was observed corresponding to the Fe_2O_3 nanoparticles (Fig. 1A). These spectral changes indicate that the supramolecular assemblies of derivative **3** interact with metal ions and serve as reactors for the reduction of metal ions into their nanoforms to generate Cu_2O–Fe_2O_3 nanohybrid materials. The colour of the solution changed from colourless to yellowish to dark brown (Fig. S14 in the ESI†).

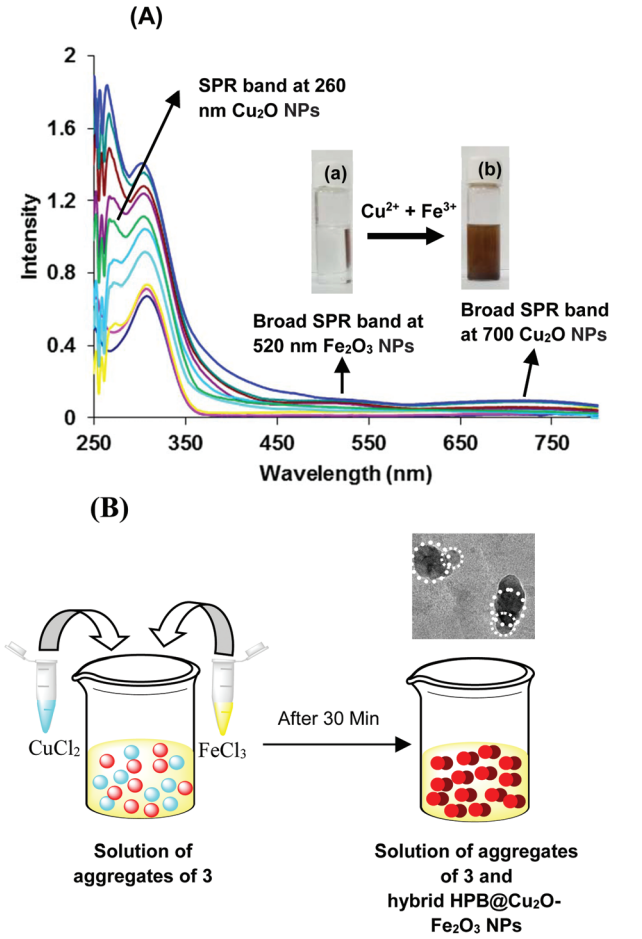

Fig. 1 (A) UV-vis spectra of derivative **3** upon addition of Cu^{2+} and Fe^{3+} ions simultaneously in the H_2O/THF (6/4) mixture. The inset figure shows the color change upon addition of Fe^{3+} and Cu^{2+} ions. (B) Schematic representation for the preparation of hybrid Cu_2O–Fe_2O_3 NPs.

Characterization of the catalytic system

The TEM studies of the supramolecular assemblies of derivative **3** in the presence of Fe^{3+} and Cu^{2+} ions showed the presence of spherical-shaped Cu_2O–Fe_2O_3 nanohybrid materials supported on the assemblies of the HPB derivative (Fig. 2A). The average size of the hybrid Cu_2O–Fe_2O_3 nanoparticles was found to be in the range of 5–7 nm. The high-resolution TEM image showed *d* spacings of 0.21 nm and 0.24 nm (ref. 45) corresponding to the (200) and (111) planes of Cu_2O NPs and *d* spacings of 0.25 and 0.27 nm (ref. 46) corresponding to the (110) and (104) planes of Fe_2O_3 NPs (Fig. 2B and C). The energy-dispersive X-ray spectroscopy (EDX) showed the presence of Fe, Cu and O elements in the nanohybrid material (Fig. S15 in the ESI†). The TEM-EDS line-scanning profile confirmed the formation of a nanohybrid of Cu_2O–Fe_2O_3 NPs (Fig. S16 in the ESI†). The DLS studies also indicated the presence of particles having an average size in the range of 5–8 nm (Fig. S17 in the ESI†). The powder X-ray diffraction (XRD) measurement showed the presence of diffraction peaks at 29.60, 36.46, 42.24, 52.64, 61.42, and 73.63 attributed to the (110), (111), (200), (211), (220) and (311) crystal planes of cubic

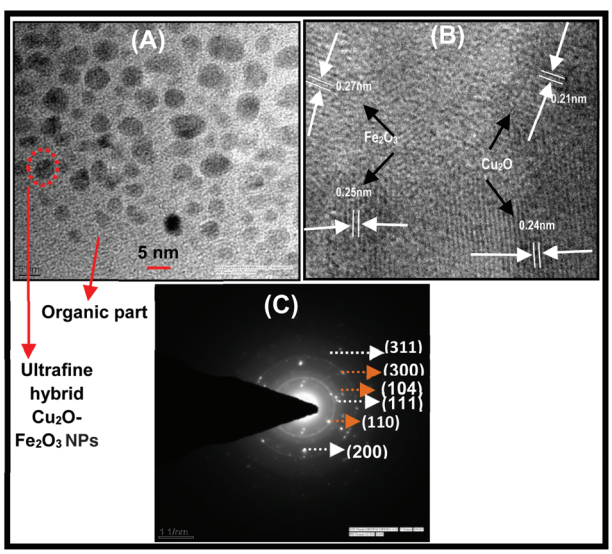

Fig. 2 (A) TEM images show ultrafine hybrid Cu_2O–Fe_2O_3 NPs deposited on the HPB derivative, (B) SAED and (C) HR TEM ultrafine hybrid Cu_2O–Fe_2O_3 NPs.

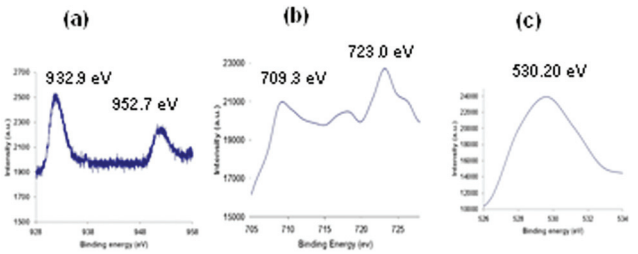

Fig. 3 (a) XPS spectrum of the Cu 2p region, (b) XPS spectrum of the Fe 2p region, and (c) XPS spectrum of the 1s region of O of ultrafine hybrid Cu_2O–Fe_2O_3 NPs.

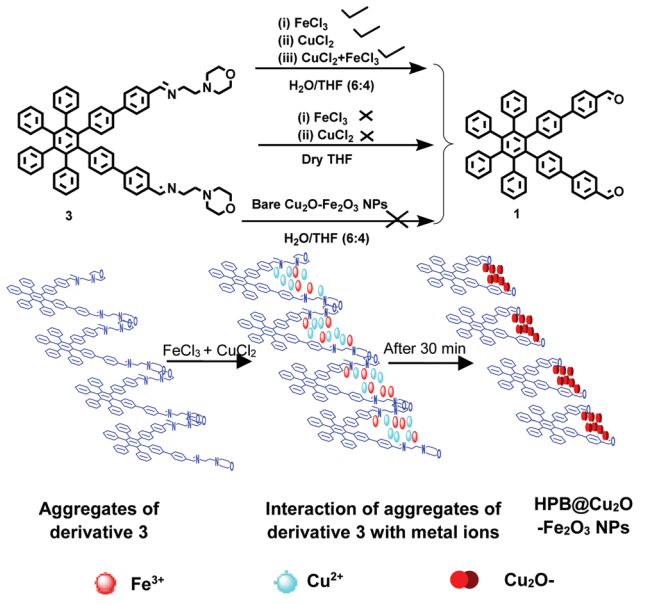

Scheme 3 Schematic representation of the preparation of hybrid Cu_2O–Fe_2O_3 NPs using the aggregates of derivative **3**.

(primitive) Cu_2O NPs, respectively. The diffraction peaks were observed at 33.40 and 35.70 (2θ) corresponding to the (104) and (110) planes of Fe_2O_3 NPs, respectively[34] (Fig. S18 in the ESI†). In the FT-IR spectrum of hybrid nanoparticles, peaks at 580 cm^{-1} corresponding to the Fe–O bond of Fe_2O_3 NPs and at 628 cm^{-1} corresponding to Cu_2O NPs were observed[47] (Fig. S19 in the ESI†). The XPS studies were further employed to investigate the compositions and elemental states of the samples. The high-resolution Cu 2p XPS spectrum (Fig. S20 in the ESI†) shows the presence of two main peaks at 932.9 and 952.7 eV, which correspond to the Cu $2p_{3/2}$ and Cu $2p_{1/2}$ spin–orbital components of Cu species, respectively (Fig. 3a). Further, the binding energies of the Fe $2p_{1/2}$ and Fe $2p_{3/2}$ are found to be 709.3 and 723 eV, respectively (Fig. 3b), which confirm the formation of Fe_2O_3 NPs. The O 1s region of the hybrid Cu_2O–Fe_2O_3 NPs is shown in Fig. 3c.[35] The super-paramagnetic nature of the hybrid Cu_2O–Fe_2O_3 NPs was observed *via* magnetic hysteresis measurements[48] (Fig. S21 in the ESI†).

To understand the mechanism of reduction of metallic species by the aggregates of derivative **3**, we performed a reaction between the Fe^{3+}, Cu^{2+} ions and supramolecular assemblies of derivative **3** in H_2O/THF (6/4, v/v) at room temperature under lab conditions. After the formation of Cu_2O–Fe_2O_3 NPs (30 min), the solution of the aggregates of derivative **3** containing the nanoparticles was slowly evaporated. After two days, brown precipitates appeared which were separated by filtration and then washed with THF. The filtrate was evaporated to obtain the solid residue. The presence of a signal at 10.00 ppm corresponding to the aldehyde proton and the absence of a signal at 8.26 ppm corresponding to the imino proton in the ^{1}H NMR spectrum of the solid residue (Fig. S22 in the ESI†) suggested the hydrolysis of imino moieties during the formation of hybrid Cu_2O–Fe_2O_3 NPs (shown in Scheme 3). Further, in the IR spectrum of the hydrolyzed species, a sharp peak was observed at 1697 cm^{-1} corresponding to the C=O stretching of the aldehyde group (Fig. S23 in the ESI†). To gain insight into the metal NP-induced cleavage of the imine linkage, we performed a series of experiments. First, we carried out a reaction between derivative **3** and metal ions (Fe^{3+} and Cu^{2+} ions) separately under lab conditions in dry THF. The absorption spectrum of the reaction mixture did not show the formation of nanoparticles upon addition of metal ion solution (Fig. S24 in the ESI†). After the usual workup, the ^{1}H NMR spectrum of the recovered compound clearly indicated the presence of derivative **3** and no formation of aldehyde was observed. These studies suggest the important role played by supramolecular aggregates in aqueous media as reactors for the generation of NPs. Afterwards, we examined the role of Fe^{3+} and Cu^{2+} ions, separately in the formation of hydrolyzed species. We performed two separate experiments in mixed aqueous media under lab conditions. Interestingly, in both the cases, cleavage of imino linkages was observed. Further, to gain more insight into the mechanism of cleavage of imine linkages (*i.e.* whether the formation of hybrid nanoparticles and cleavage of imine linkages is a simultaneous process or the cleavage is induced by alloy NPs), we prepared bare Cu_2O–Fe_2O_3 NPs and performed the same reaction in mixed aqueous media in the presence of these NPs. Amazingly, bare Cu_2O–Fe_2O_3 NPs could not cleave the imine linkages. These observations clearly suggest that the formation of hybrid Cu_2O–Fe_2O_3 NPs and the cleavage of the imine linkages go side by side. Next, we examined the photophysical behaviour of derivative **1** in the H_2O/THF (6 : 4) mixture. Derivative **1** showed an emission band at 455 nm. Upon addition of bare hybrid NPs, the emission intensity of the solution of derivative **1** decreased by 74% (Fig. S25 in the ESI†). Further, a good spectral overlap was observed between the fluorescence emission spectrum of derivative **1** and the absorption spectrum of Cu_2O–Fe_2O_3 NPs, which suggests the possibility of energy transfer between hydrolyzed species **1** and Cu_2O–Fe_2O_3 NPs (Fig. S26 in the ESI†).

Photocatalytic activity of the ultrafine hybrid Cu_2O–Fe_2O_3 NPs for the Ullmann–Goldberg coupling

The possibility of energy transfer between the supramolecular assemblies and nanoparticles prompted us to investigate the catalytic efficiency of the as-prepared hybrid catalytic system in the Ullmann–Goldberg coupling reaction under visible light irradiation. The reaction between iodobenzene (**4a**, 0.4 mmol) and morpholine (**5**, 2 mmol) in the H_2O/EtOH (1 : 1) solvent mixture in the presence of 0.5 mol% hybrid HPB@Cu_2O–Fe_2O_3 nanoparticles under aerial conditions and visible light irradiation was screened as the model reaction. To our delight, the reaction was complete in six hours and the desired product **6** was obtained in 90% yield (Table 1, entry 1). Next, we repeated the model reaction in different solvents such as triethylene glycol (TEG), glycerol, EtOH, water and the EtOH : H_2O mixture (Table 1, entries 1–5). The desired product was obtained in comparable yields in all these solvents; however, the yield of the final product was low in aqueous media. Thus, we chose H_2O : EtOH (1 : 1) as the reaction medium for carrying out further reactions. Further, we also investigated the effect of various bases such as K_2CO_3, Cs_2CO_3 and *t*-BuOK on the photocatalytic efficiency of the Ullmann–Goldberg coupling reaction (Table 1, entries 6 and 7). Interestingly, switching of the base has no significant effect on the yield of the reaction; however, in the absence of alkaline conditions, the desired product was obtained only in traces (Table 1, entry 8). Thus, a basic medium is essential for carrying out the reaction. We chose K_2CO_3 as the base due to its more availability and economic viability. We also performed the model reaction under dark conditions and the coupled product was obtained in traces (Table 1, entry 9). This study clearly emphasizes the important role of visible radiation in the feasibility of the reaction. Further, to understand the role of supramolecular assemblies along with hybrid Cu_2O–Fe_2O_3 nanoparticles in the Ullmann–Goldberg coupling, we prepared bare Cu_2O NPs,[49] bare Fe_2O_3 NPs[50] and bare Cu_2O–Fe_2O_3 NPs[34] by hydrothermal methods. We evaluated the catalytic efficiency of these metal nanoparticles in the C–N coupling of iodobenzene and morpholine under visible light. The desired product was obtained in 30% yield in the presence of Cu_2O NPs, 20% yield in the presence of Fe_2O_3 NPs and 32% yield in the presence of Cu_2O–Fe_2O_3 NPs (Table 1, entries 10–12). The above results highlight the important contribution of supramolecular assemblies towards the catalytic efficiency of hybrid Cu_2O–Fe_2O_3 NPs in the coupling reaction. We also carried out the model reaction in the presence of the aggregates of HPB derivative **1**, but the reaction did not proceed (Table 1, entry 13). This result shows that the hybrid Cu_2O–Fe_2O_3 nano-composite is the catalytic center. Further, the reaction in the presence of the assemblies of derivative **1** and bare Cu_2O–Fe_2O_3 NPs furnished the desired product only in 25% yield (Table 1, entry 14).

Next, we investigated the effect of the halide (Br and Cl) leaving group on the progress of the reaction. Interestingly, in the presence of hybrid HPB@Cu_2O–Fe_2O_3 NPs as a catalyst, the Ullmann–Goldberg coupling involving bromobenzene and chlorobenzene went smoothly to yield the products (Scheme 4) in high yields. In the case of bromobenzene, the product was obtained in 85% yield, while the yield was reduced to 70% in the case of chlorobenzene.

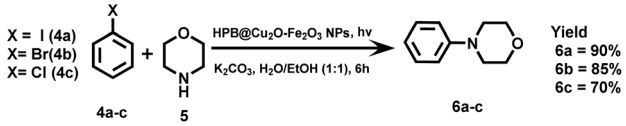

Scheme 4 C–N coupling reaction between aryl halides and morpholine in H_2O/EtOH (1 : 1), using hybrid HPB@Cu_2O–Fe_2O_3 NPs under visible light irradiation.

Table 1 Optimization of the reaction conditions for the model reaction between iodobenzene and morpholine

Entry	Catalytic system	Time (h)	Base	Solvent	Light/dark	Isolated yield
1	HPB@Cu_2O–Fe_2O_3 NPs	6	K_2CO_3	H_2O/EtOH (1 : 1)	Light	90%
2	HPB@Cu_2O–Fe_2O_3 NPs	6	K_2CO_3	EtOH	Light	92%
3	HPB@Cu_2O–Fe_2O_3 NPs	6	K_2CO_3	Triethylene glycol	Light	80%
4	HPB@Cu_2O–Fe_2O_3 NPs	6	K_2CO_3	Glycerol	Light	83%
5	HPB@Cu_2O–Fe_2O_3 NPs	10	K_2CO_3	H_2O	Light	65%
6	HPB@Cu_2O–Fe_2O_3 NPs	6	Cs_2CO_3	H_2O/EtOH (1 : 1)	Light	90%
7	HPB@Cu_2O–Fe_2O_3 NPs	6	*t*-BuOK	H_2O/EtOH (1 : 1)	Light	90%
8	HPB@Cu_2O–Fe_2O_3 NPs	8	—	H_2O/EtOH (1 : 1)	Light	Traces
9	HPB@Cu_2O–Fe_2O_3 NPs	24	K_2CO_3	H_2O/EtOH (1 : 1)	Dark	Traces
10	Bare Cu_2O	6	K_2CO_3	H_2O/EtOH (1 : 1)	Light	30%
11	Bare Fe_2O_3	6	K_2CO_3	H_2O/EtOH (1 : 1)	Light	20%
12	Bare bimetallic Cu_2O–Fe_2O_3 NPs	6	K_2CO_3	H_2O/EtOH (1 : 1)	Light	32%
13	HPB derivative **1** (hydrolyzed species)	6	K_2CO_3	H_2O/EtOH (1 : 1)	Light	No reaction
14	HPB derivative **1** (hydrolyzed species) and bare Cu_2O–Fe_2O_3	6	K_2CO_3	H_2O/EtOH (1 : 1)	Light	25%

Next, we examined the substrate scope with regard to various aryl halides and cyclic amines under the optimized reaction conditions. We carried out the reaction between substituted aryl halides and morpholine(**5**)/piperidine(**9**)/pyrrolidine(**10**) in the presence of hybrid HPB@Cu_2O–Fe_2O_3 NPs (Scheme 5). Aryl halides having electron-donating and electron-withdrawing groups furnished the desired products in excellent yields. Both substituted aryl iodides and aryl bromides worked well under the optimized reaction conditions. These results show that the as-prepared hybrid HPB@Cu_2O–Fe_2O_3 NPs act as an efficient and greener catalytic system for carrying out the Ullmann–Goldberg reaction under visible light irradiation.

Further, different substituted aryl iodides were successfully treated with an aqueous solution of NH_3 (**14**) to obtain the corresponding substituted anilines in high yields under the optimized reaction conditions (Scheme 6; **18a–18d**). The efficiency of the hybrid HPB@Cu_2O–Fe_2O_3 NPs toward different primary and secondary aliphatic amines was also investigated. To our delight, the C–N coupling of aryl iodides with primary aliphatic amines such as *n*-butylamine (**15**), *n*-octylamine (**16**) and secondary 2-aminooctylamine (**17**) furnished *N*-arylated amines in excellent yields (Scheme 6; **19**, **20a–c**, and **21**).

The Ullmann–Goldberg coupling reaction using hybrid HPB@Cu_2O–Fe_2O_3 NPs was further extendable to primary and secondary aromatic amines. We carried out the reactions between aniline (**22**) and diphenylamine (**23**) with aryl iodides under the optimized reaction conditions. The substituted diphenylamines and triphenylamines were furnished in good to excellent yields (Scheme 7).

Next, we examined the reactivity of N-heterocyclic amines toward aryl halides in the presence of hybrid HPB@Cu_2O–Fe_2O_3 NPs. We carried out the Ullmann–Goldberg coupling

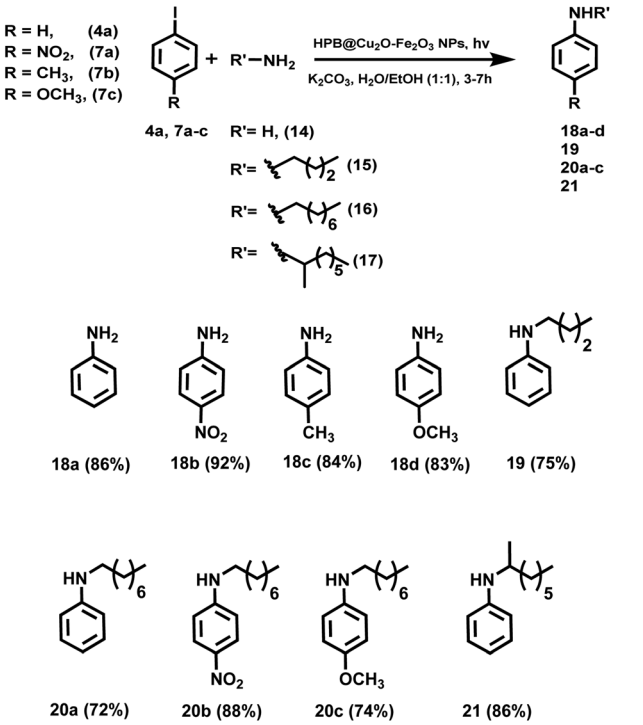

Scheme 6 C–N coupling reaction between substituted aryl iodides and ammonia/aliphatic amines in H_2O/EtOH (1 : 1), using hybrid HPB@Cu_2O–Fe_2O_3 NPs under visible light irradiation.

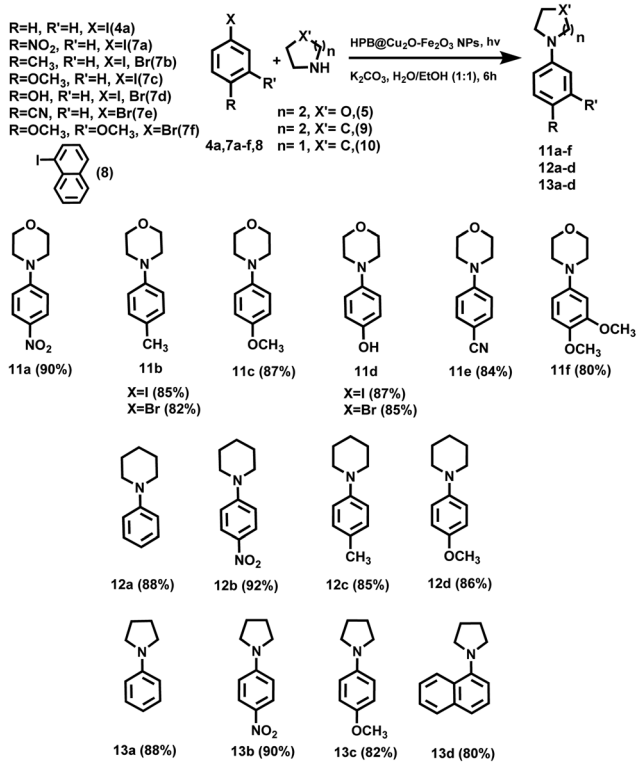

Scheme 5 C–N coupling reaction between substituted aryl halides and cyclic amines in H_2O/EtOH (1 : 1), using hybrid HPB@Cu_2O–Fe_2O_3 NPs under visible light irradiation.

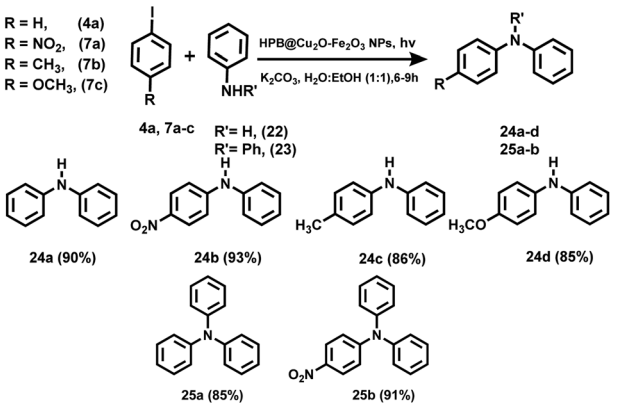

Scheme 7 C–N coupling reaction between substituted aryl iodides and aniline/diphenylamine in H_2O/EtOH (1 : 1), using hybrid HPB@Cu_2O–Fe_2O_3 NPs under visible light irradiation.

reaction between carbazole (**26**) and various substituted aryl iodides under the optimized reaction conditions. Interestingly, *N*-substituted carbazole derivatives having electron-donating and electron-withdrawing groups were obtained in good yields (Scheme 8). Recently, the synthesis of *N*-substituted carbazole derivatives has been catalyzed by an iridium-based photocatalytic system in the presence of a copper salt and LiO^tBu under blue LED irradiation in DMSO as the reaction media.[22] On the other hand, hybrid HPB@Cu_2O–Fe_2O_3 NPs act as a sustainable and reusable photocatalytic system for the synthesis of *N*-substituted carbazole under mild conditions to afford the target derivative in high yield.

We also examined the photocatalytic efficiency of hybrid HPB@Cu_2O–Fe_2O_3 NPs in the reaction between heteroaryl bromide (**28**) and carbazole (**26**). The reaction was complete in 13 h under the optimized reaction conditions to furnish the target compound in good yield (Scheme 9).

Further, the hybrid HPB@Cu_2O–Fe_2O_3 NPs were utilized in the reaction between indole (**30**) and substituted aryl iodides. The reaction was complete in 10 h and the desired products were obtained in good yields (Scheme 10). Interestingly, *N*-substituted indole **31b** having an electron-withdrawing group (–NO_2) was obtained in a higher yield in comparison with indoles **31a** and **31c** having neutral and electron-donating groups.

Inspired by these results, we checked the catalytic efficiency of the hybrid HPB@Cu_2O–Fe_2O_3 NPs in the reaction of 1-iodo-4-nitrobenzene (**7a**) with other N-heterocyclic amines such as

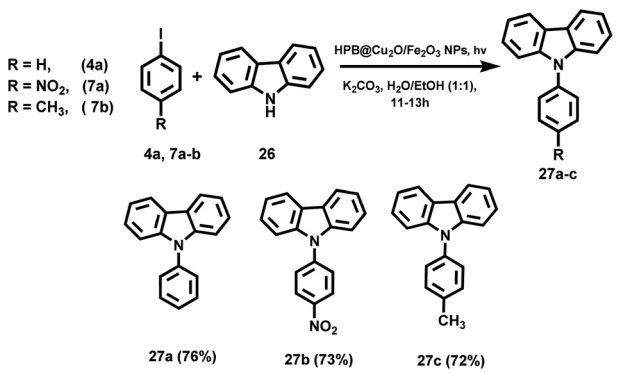

Scheme 8 C–N coupling reaction between substituted aryl iodides and carbazole H_2O/EtOH (1 : 1), using hybrid HPB@Cu_2O–Fe_2O_3under visible light irradiation.

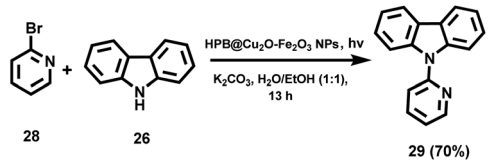

Scheme 9 C–N coupling reaction between 2-pyridinyl bromide and carbazole in H_2O/EtOH (1 : 1), using hybrid HPB@Cu_2O–Fe_2O_3 NPs under visible light irradiation.

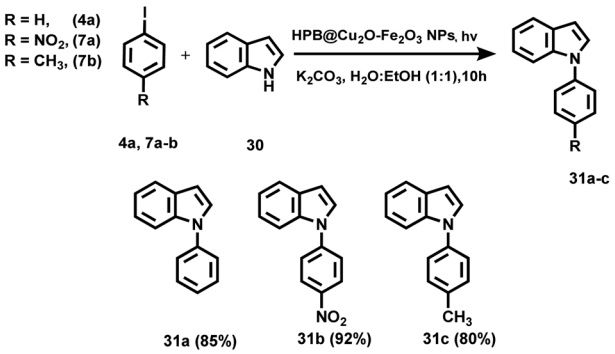

Scheme 10 C–N coupling reaction between substituted aryl iodides and indole in H_2O/EtOH (1 : 1), using hybrid HPB@Cu_2O–Fe_2O_3 NPs under visible light irradiation.

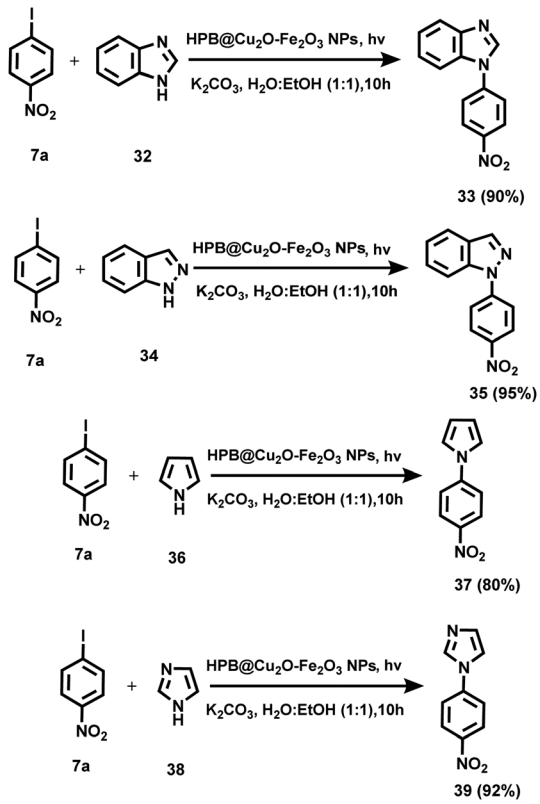

Scheme 11 C–N coupling reaction between 1-iodo-4-nitrobenzene and different N-heterocyclic amines in H_2O/EtOH (1 : 1), using hybrid HPB@Cu_2O–Fe_2O_3 NPs under visible light irradiation.

benzimidazole (**32**), indazole (**34**), pyrrole (**36**) and imidazole (**38**). The desired products were furnished in excellent yields under the optimized reaction conditions (Scheme 11).

We also examined the applicability of the as-prepared hybrid HPB@Cu_2O–Fe_2O_3 NPs for the synthesis of derivative **41**, which is an important precursor of different materials having applications in the OLED industry. The reaction between the pyrazine derivative (**40**) and carbazole (**26**) in the presence of the as-prepared catalytic system in mixed aqueous

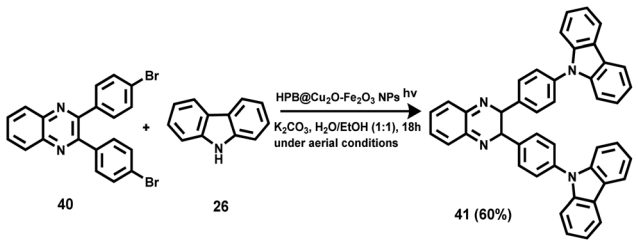

Scheme 12 C–N coupling reaction between the derivatives of pyrazine and carbazole in H_2O/EtOH (1 : 1), using hybrid HPB@Cu_2O–Fe_2O_3 NPs under visible light irradiation.

media furnished the desired product in 60% yield (Scheme 12) (Fig. S44 and S45 in the ESI†). Earlier, this compound had been synthesized using palladium acetate as a catalyst under an inert atmosphere at a high temperature (140 °C) in the presence of DMSO as the solvent.[51]

Further, we chose the reaction between iodobenzene **5a** and morpholine **6** as the model reaction to examine the recyclability of the photocatalytic system. The as-prepared hybrid HPB@Cu_2O–Fe_2O_3 NPs could be easily separated from the aqueous layer of the reaction mixture by simple magnetic separation and the isolated catalytic system was reused up to six times. After the sixth cycle, the yield of the final product reduced to 70% (Fig. 4). The TEM image of the recycled catalytic system showed a change in the size and morphology of the hybrid NPs (Fig. S27 in the ESI†). We also carried out atomic absorption studies (AAS) of the residual liquid left after the recycling of the catalyst and found that only 1.91 ppm of Cu had leached into the solution.

Mechanism of the photocatalytic Ullmann–Goldberg coupling catalyzed by ultrafine hybrid HPB@Cu_2O–Fe_2O_3 NPs

To understand the mechanism of C–N coupling reaction catalyzed by hybrid HPB@Cu_2O–Fe_2O_3 NPs, we investigated the model reaction of **4a** with **5** in the presence of the radical scavenger 2,2,6,6-tetramethyl-1-piperidinoxyl (TEMPO, 2 equiv.). The presence of TEMPO completely inhibited the reaction. The ESI MS studies of the reaction mixture suggested the formation of an adduct between benzene and TEMPO (Fig. S28 in the ESI†). These studies support the radical mechanism for the reaction as shown in Scheme 13.

Further, we also prepared a 'dip strip' by dip coating a filter paper strip in the catalytic solution. The SEM image of the

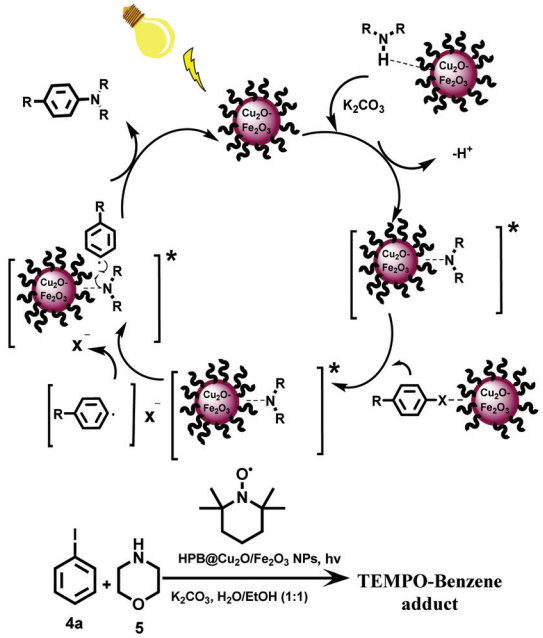

Scheme 13 Proposed mechanism of photocatalytic C–N coupling catalyzed by HPB@Cu_2O–Fe_2O_3 NPs (irradiation with a 60 W tungsten filament bulb).

strip clearly shows the deposition of the supramolecular ensemble on the filter paper (Fig. S29 in the ESI†). The EDX pattern of the dip-coated paper strip also confirmed the deposition of the hybrid HPB@Cu_2O–Fe_2O_3 NPs (Fig. S30 in the ESI†). The as-prepared coated filter paper strip was used as a heterocatalytic system for carrying out the reaction between iodobenzene (**4a**) and morpholine (**5**). To our delight, the reaction was complete in 7 h to furnish the desired product in 86% yield. After the completion of the reaction, the coated paper strip was removed from the reaction mixture, air dried and reused as a catalytic system for the second run by following the same procedure. The coated paper strip could be reused up to three cycles for carrying out the C–N coupling reaction and after the 3rd cycle the desired product was furnished in 65% yield (Fig. 5). The SEM image and EDX profile of the paper strip after the 3rd cycle showed a decrease in the coated area of the paper strip (Fig. S31 and S32 in the ESI†). We believe that the partial removal of the coated material

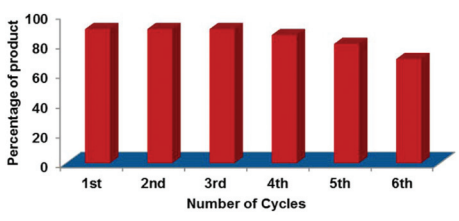

Fig. 4 Recyclability of hybrid HPB@Cu_2O-Fe_2O_3 NPs for carrying out C–N coupling reaction between morpholine and iodobenzene.

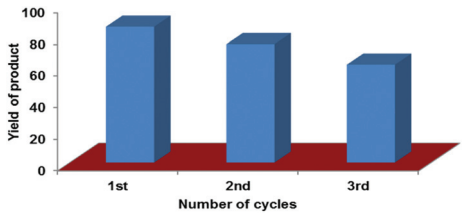

Fig. 5 Recyclability of the dip-coated paper strip with hybrid HPB@Cu_2O–Fe_2O_3 NPs for carrying out C–N coupling reaction between morpholine and iodobenzene under visible light.

during the recyclability experiment is the reason behind the decreased efficiency of the catalytic system.

Conclusion

A HPB-based derivative **3** has been designed and synthesized, which forms supramolecular assemblies in aqueous media. The supramolecular assemblies of derivative **3** act as nanoreactors and stabilizers for the synthesis of ultrafine hybrid HPB@Cu_2O–Fe_2O_3 NPs without using any reducing and capping agents in mixed aqueous media at room temperature. The ultrafine hybrid HPB@Cu_2O–Fe_2O_3 NPs serve as an efficient, recyclable photocatalytic system for carrying out C–N coupling between substituted aryl halides and various primary/secondary aliphatic, aromatic and N-heterocyclic amines at room temperature in the mixed aqueous media under visible light irradiation and aerial conditions. The ultrafine hybrid HPB@Cu_2O–Fe_2O_3 NPs act as a green photocatalytic system for the synthesis of medicinally important *N*-substituted carbazole derivatives. The use of visible light as an energy source to carry out C–N coupling reactions over thermal conditions makes this approach greener and sustainable. Further, the as-prepared coated filter paper strip was used as a heterocatalytic system for carrying out C–N bond formation reactions with reusability up to three cycles.

Experimental section

General experimental methods and materials[52]

The general experimental methods, quantum yield calculations, and materials used are the same as those reported earlier by us.

UV-vis and fluorescence titrations[52]

A 10^{-3} (M) stock solution of compound **3** was prepared by dissolving 9.67 mg of compound **3** in 10.0 ml of THF. 15 μl of this stock solution was further diluted with 1800 μl water (pH = 7.05) to prepare a 3.0 ml solution of derivative **3** (5.0 μM) and this solution was used for each UV-vis and fluorescence experiment. The aliquots of freshly prepared standard solutions of metal perchlorates [M(ClO_4)X; M = Zn^{2+}, Cu^{2+}, Hg^{2+}, Au^{3+}, Fe^{2+}, Fe^{3+}, Co^{2+}, Pb^{2+}, Pd^{2+}, Ni^{2+}, Cd^{2+}, Ba^{2+}, Mg^{2+}, Ag^{+}, and Al^{3+}; X = 1–3], chlorides (MClY; Y = 1–3) and $CuCl_2$ (10^{-1} M to 10^{-3} M) in distilled water were added to the 3.0 ml solution of compound **3** taken in a quartz cuvette and their spectra were recorded.

Synthesis of hybrid HPB@Cu_2O–Fe_2O_3 NPs

The hybrid HPB@Cu_2O–Fe_2O_3 NPs were prepared by adding an aqueous solution of 180 μL of $CuCl_2$ (10^{-2} M) and 90 μL of $FeCl_3$ (10^{-2} M) to 3.0 ml of 5 μM solution of derivative **3** in a H_2O : THF (6 : 4) solvent mixture. The resulting solution was stirred at room temperature. The solution turned dark brown after 30 min. 0.5 mol% of this solution was used as such in each catalytic experiment.

Synthesis of derivative 3

A clear solution of derivative **1** (0.1 g, 0.13 mmol) and 4-(2-aminoethyl)morpholine **2** (0.035 g, 0.27 mmol) in dry dichloromethane (DCM)/ethanol (EtOH) (2 : 8) was refluxed at 70 °C. After the completion of the reaction, precipitates were formed (48 h) which were filtered and recrystallized from methanol to afford the white compound **3** in 78% yield; mp: >250 °C; ^{1}H NMR (300 MHz, $CDCl_3$) δ = 8.26 (s, 2H, HC═N), 7.66 (d, J = 6 Hz, 4H, Ar–H), 7.47 (d, J = 6 Hz, 4H, Ar–H), 7.17 (d, J = 9 Hz, 4H, Ar–H), 6.94 (d, J = 9 Hz, 4H, Ar–H), 6.86–6.85 (m, 20H, Ar–H), 3.78–3.69 (m, 12H, CH_2), 2.70 (t, J = 7.5 Hz, 4H, CH_2), 2.54 (t, J = 4.5 Hz, 8H, CH_2), ^{13}C NMR ($CDCl_3$, 125 MHz) δ = 161.63, 142.97, 140.63, 140.34, 140.51, 139.76, 136.73, 134.74, 131.97, 131.39, 128.33, 126.85, 126.70, 126.60, 125.26, 66.99, 59.34, 59.09, 54.04; mass m/z = 967.4964 $[M + 1]^+$.

General procedure for the photocatalytic Ullmann–Goldberg coupling between aryl-halide and cyclic/acyclic amines catalyzed by hybrid HPB@Cu_2O–Fe_2O_3 NPs

A mixture of aryl-halide (0.4 mmol), amine (2 mmol) and K_2CO_3 (1 mmol) in H_2O : EtOH (1 : 1) in the presence of hybrid HPB@Cu_2O–Fe_2O_3 NPs (0.5 mol%) as a photocatalyst was stirred at room temperature for 3–9 h under visible light. After the completion of the reaction (monitored by TLC), the organic part was extracted with $CHCl_3$ and the combined organic layer was dried over anhydrous sodium sulphate and distilled under reduced pressure. Products **11a–e** were purified by recrystallization from a methanol/hexane(1 : 5) mixture. In the case of other cyclic, acyclic aliphatic and aromatic amine derivatives, the products (**11f**, **12a–d**, **13a–d**, **18a–d**, **19**, **20a–c**, **21**, **24a–d**, and **25a–b**) were purified by column chromatography on silica gel. All the products were identified by ^{1}H NMR spectroscopy (Fig. S33–S61 in the ESI†).

General procedure for the photocatalytic Ullmann–Goldberg coupling reaction between aryl halide and N-heterocyclic amines catalyzed by hybrid HPB@Cu_2O–Fe_2O_3 NPs

A mixture of arylhalides (0.4 mmol), N-heterocyclic amines (2 mmol) and K_2CO_3 (1 mmol) in H_2O : EtOH (1 : 1) in the presence of HPB@Cu_2O–Fe_2O_3 NPs (0.5 mol%) as a photocatalyst was stirred at room temperature for 10–13 h under visible light. After the completion of the reaction (monitored by TLC), the organic part was extracted with $CHCl_3$ and the organic layer was dried over anhydrous sodium sulphate and distilled under reduced pressure to give a solid residue. The products (**27a–c**, **29**, **31a**, and **31c**) were purified by column chromatography on silica gel using EtOAc : hexane (1 : 19) as an eluent, while nitroderivatives (**31b**, **33**, **35**, **37**, and **39**) were purified by recrystallization from hexane. All the products were identified by ^{1}H NMR spectroscopy (Fig. S62–S72 in the ESI†).

Procedure for the synthesis of derivative 41

A mixture of derivative **40** (0.4 mmol), carbazole (**26**) (2 mmol) and K_2CO_3 (1 mmol) in H_2O : EtOH (1 : 1) in the presence of hybrid HPB@Cu_2O–Fe_2O_3 NPs (0.5 mol%) as a photocatalyst was stirred for 18 h at room temperature under visible light. After the completion of the reaction (monitored by TLC), the organic part was extracted with $CHCl_3$ and the organic layer was dried over anhydrous sodium sulphate and distilled under reduced pressure to give a solid residue. The product (**41**) was purified by column chromatography on silica gel using EtOAc : hexane(1 : 19) as an eluent. All the products were identified by ^{1}H NMR spectroscopy (Fig. S73 and S74 in the ESI†).

Conflicts of interest

There are no conflicts to declare.

Acknowledgements

V. B. is thankful to the Science and Engineering Research Board (SERB), New Delhi (ref. no. EMR/2014/000149) for financial support. We are also thankful to the UGC (New Delhi) for "University with Potential for Excellence" (UPE) and DST for the FIST programme.

References

1 J.-P. Corbet and G. Mignani, *Chem. Rev.*, 2006, **106**, 2651.
2 B. Schlummer and U. Scholz, *Adv. Synth. Catal.*, 2004, **346**, 1599.
3 D. S. Surry and S. L. Buchwald, *Chem. Sci.*, 2011, **2**, 27.
4 J. F. Hartwig, *Nature*, 2008, **455**, 314.
5 J. Bariwal and E. Van der Eycken, *Chem. Soc. Rev.*, 2013, **42**, 9283.
6 F. Paul, J. Patt and J. Hartwig, *J. Am. Chem. Soc.*, 1994, **116**, 5969.
7 Q. Xiao, S. Sarina, A. Bo, J. Jia, H. Liu, D. P. Arnold, Y. Huang, H. Wu and H. Zhu, *ACS Catal.*, 2014, **4**, 1725.
8 Y. Zhang, X. Yang, Q. Yao and D. Ma, *Org. Lett.*, 2012, **14**, 3056.
9 J. Gao, S. Bhunia, K. Wang, L. Gan, S. Xia and D. Ma, *Org. Lett.*, 2017, **19**, 2809.
10 W. Zhou, M. Fan, J. Yin, Y. Jiang and D. Ma, *J. Am. Chem. Soc.*, 2015, **137**, 11942.
11 L. Zhou, M. Yin, X. Jiang, Q. Huang and W. Lang, *New J. Chem.*, 2016, **40**, 1454.
12 E. B. Corcoran, M. T. Pirnot, S. Lin, S. D. Dreher, A. D. DiRocco, I. W. Davies, S. L. Buchwald and D. W. C. MacMillan, *Science*, 2016, **353**, 279.
13 F. Heshmatpour and R. Abazari, *RSC Adv.*, 2014, **4**, 55815.
14 H.-P. Gong, Z.-J. Quan and X.-C. Wang, *Appl. Organomet. Chem.*, 2016, **30**, 949.
15 Y.-C. Teo and G.-L. Chua, *Chem. – Eur. J.*, 2009, **15**, 3072.
16 B. Y.-H. Tan and Y.-C. Teo, *Org. Biomol. Chem.*, 2014, **12**, 7478.
17 G. Toma and R. Yamaguchi, *Eur. J. Org. Chem.*, 2010, 6404.
18 N. Mukherjee, T. Chatterjee and B. C. Ranu, *Eur. J. Org. Chem.*, 2015, 4018.
19 H. Ibrahim and M. D. Bala, *J. Organomet. Chem.*, 2015, **794**, 301.
20 R. Ayothiraman, S. Rangaswamy, P. Maity, E. M. Simmons, G. L. Beutner, J. Janey, D. S. Treitler, M. D. Eastgate and R. Vaidyanathan, *J. Org. Chem.*, 2017, **82**, 7420.
21 D. S. Surry and S. L. Buchwald, *Chem. Sci.*, 2010, **1**, 13.
22 W.-J. Yoo, T. Tsukamoto and S. Kobayashi, *Org. Lett.*, 2015, **17**, 3640.
23 H. Deol, S. Pramanik, M. Kumar, I. A. Khan and V. Bhalla, *ACS Catal.*, 2016, **6**, 3771.
24 M. Kaur, S. Pramanik, M. Kumar and V. Bhalla, *ACS Catal.*, 2017, **7**, 2007.
25 R. Chopra, K. Sharma, M. Kumar and V. Bhalla, *J. Org. Chem.*, 2016, **81**, 1039.
26 S. Kaur, M. Kumar and V. Bhalla, *Chem. Commun.*, 2015, **51**, 16327.
27 S. Pramanik, V. Bhalla and M. Kumar, *Chem. Commun.*, 2014, **50**, 13533.
28 F. Y. Kwong, A. Klapars and S. L. Buchwald, *Org. Lett.*, 2002, **4**, 581.
29 S. Pramanik, H. Deol, V. Bhalla and M. Kumar, *ACS Appl. Mater. Interfaces*, 2018, **10**, 12112.
30 G. Singh, S. I. Reja, V. Bhalla, D. Kaur, P. Kaur, S. Arora and M. Kumar, *Sens. Actuators, B*, 2017, **249**, 311.
31 R. Chopra, M. Kumar and V. Bhalla, *Chem. Commun.*, 2016, **52**, 10179.
32 D. Guo, H. Huang, J. Xu, H. Jiang and H. Liu, *Org. Lett.*, 2008, **10**, 4513.
33 A. R. Shaikh, R. Sahnoun, E. Broclawik, M. Koyama, H. Tsuboi, N. Hatakeyama, A. Endou, H. Takaba, M. Kubo, C. A. Del Carpio and A. Miyamoto, *J. Inorg. Biochem.*, 2009, **103**, 20.
34 S. K. Lakhera, R. Venkataramana, A. Watts, M. Anpo and B. Neppolian, *Res. Chem. Intermed.*, 2017, **43**, 5091.
35 P. Mirtchev, K. Liao, E. Jaluague, Q. Qiao, Y. Tian, M. Varela, K. S. Burch, S. J. Pennycook, D. D. Perovic and G. Ozin, *J. Mater. Chem. A*, 2014, **2**, 8525.
36 N. Tsukada, N. Ohnishi, S. Aono and F. Takahashi, *Organometallics*, 2012, **31**, 7336.
37 S. Urgaonkar, J.-H. Xu and J. G. Verkade, *J. Org. Chem.*, 2003, **68**, 8416.
38 T. Kubo, C. Katoh, K. Yamada, K. Okano, H. Tokuyama and T. Fukuyama, *Tetrahedron*, 2008, **64**, 11230.
39 A. Shafir and S. L. Buchwald, *J. Am. Chem. Soc.*, 2006, **128**, 8742.
40 K. Sharma, G. Singh, G. Singh, M. Kumar and V. Bhalla, *RSC Adv.*, 2015, **5**, 25781.
41 V. Vij, V. Bhalla and M. Kumar, *ACS Appl. Mater. Interfaces*, 2013, **5**, 5373.
42 G. G. Khan, D. Sarkar, A. K. Singh and K. Mandal, *RSC Adv.*, 2013, **3**, 1722.

43 B. Dutta, E. Kar, N. Bose and S. Mukherjee, *RSC Adv.*, 2015, **5**, 105422.
44 H. Jing, N. Large, Q. Zhang and H. Wang, *J. Phys. Chem. C*, 2014, **118**, 19948.
45 L. Chen, Y. Zhang, P. Zhu, F. Zhou, W. Zeng, D. D. Lu, R. Sun and C. Wong, *Sci. Rep.*, 2015, **5**, 9672.
46 G. Zhou, D.-W. Wang, P.-X. Hou, W. Li, N. Li, C. Liu, F. Li and H.-M. Cheng, *J. Mater. Chem.*, 2012, **22**, 17942.
47 A. B. Raut and B. M. Bhanage, *ChemistrySelect*, 2017, **2**, 10055.
48 M. Tadic, M. Panjan, V. Damnjanovic and I. Milosevic, *Appl. Surf. Sci.*, 2014, **320**, 183.
49 L. Xiong, H. Yu, C. Nie, Y. Xiao, Q. Zeng, G. Wang, B. Wang, H. Lv, Q. Li and S. Chen, *RSC Adv.*, 2017, **7**, 51822.
50 M. Lin, L. Tng, T. Lim, M. Choo, J. Zhang, H. R. Tan and S. Bai, *J. Phys. Chem. C*, 2014, **118**, 10903.
51 M. Naoki and O. Yohei, *JP* 2017155033, 2017.
52 S. Pramanik, V. Bhalla and M. Kumar, *ACS Appl. Mater. Interfaces*, 2014, **6**, 5930.